ACADEMIC PRESS

Available online at www.sciencedirect.com

SCIENCE DIRECT®

Journal of Solid State Chemistry 170 (2003) 361–367

JOURNAL OF SOLID STATE CHEMISTRY

http://elsevier.com/locate/jssc

Charge–orbital ordering above room temperature in the 2D $Pr_{1-x}Ca_{1+x}MnO_4$ manganites

M. Ibarra, R. Retoux,* M. Hervieu, C. Autret, A. Maignan, C. Martin, and B. Raveau

Laboratoire CRISMAT, Université de Caen, ISMRA CNRS- UMR-6508, 6 Boulevard du Maréchal Juin, Caen 14050 Cedex, France

Received 27 July 2002; received in revised form 27 September 2002; accepted 7 October 2002

Abstract

The investigation of the $n=1$ member of the Ruddlesden Popper family, $Pr_{1-x}Ca_{1+x}MnO_4$, using electron microscopy, transport and magnetic measurements shows that these 2D manganites exhibit long-range charge–orbital ordering over a wide composition range ($0.50 \leqslant x \leqslant 0.80$). These oxides show a remarkably high T_{CO} temperature depending on the x value, up to 330 K, the highest that has been observed to date in 2D manganites. They are characterized by the appearance of a smooth structural transition from P- to C-type inside the charge-ordered state. The high-resolution electron microscopy images of $Pr_{0.5}Ca_{1.5}MnO_4$ registered at room temperature evidence a system of double stripes similar to those observed for $Bi_{0.5}Sr_{0.5}MnO_3$, suggesting that double stripes of one sort of manganese alternate with double or quadruple stripes of a second sort of manganese.

Keywords: Ruddlesden Popper phases; Mangonites; Electron Microscopy; Charge Orbital Ordering; Magnetic properties

1. Introduction

The numerous studies carried out in the recent years on tridimensional perovskite manganites $(Ln, A)_1MnO_3$ have shown that the appearance of the colossal magnetoresistance (CMR) effect in these oxides is closely related to the presence of a charge-ordered state and to its metastable character. In contrast, for the 2D Ruddlesden Popper (RP) phases $(Ln,A)_2MnO_4$, which consist of an intergrowth of single perovskite and single rock-salt-type layers, charge–orbital ordering seems to play a different role. It was indeed shown that the manganites $La_{1-x}Sr_{1+x}MnO_4$, which are charge ordered for $x=0.50$, exhibit only a spin-glass insulating state [1,2], the ferromagnetic contribution being weakened by a decrease of their e_g bandwidth. Similarly, the antiferromagnetic state observed for $Nd_{1-x}Sr_{1+x}MnO_4$ seems to be closely related to charge-orbital ordering that appears below 270 K [3].

Very few investigations have been carried out about charge ordering in 2D manganites containing small A-site cations [4]. Recently, we showed that $Pr_{0.25}Ca_{1.75}MnO_4$ exhibits charge ordering below $T_{CO}=275$ K, with an incommensurate structure characterized by a modulation vector $q=0.28\vec{c}$ [5]. Starting from these results, we have revisited the Mn^{4+}- rich side of the 2D manganites $Pr_{1-x}Ca_{1+x}MnO_4$ ($0.50 \leqslant x \leqslant 1$). In the present paper, we show that these 2D manganites exhibit charge-orbital ordering over a wide compositional range ($0.50 \leqslant x < 0.80$) close to or above room temperature, the oxide $Pr_{0.33}Ca_{1.67}MnO_4$ having the highest $T_{CO} \approx 330$ K, that is known to date in such bidimensional systems. A detailed electron diffraction investigation shows that the charge-ordered phase $Pr_{0.50}Ca_{1.50}MnO_4$ ($x=0.50$) exhibits at low temperature a smooth structural transition from a P-type to C-type symmetry, whereas high-resolution electron microscopy (HREM) investigations at room temperature show that charge–orbital ordering appears in the form of stripes.

2. Experimental section

Ten $Pr_{1-x}Ca_{1+x}MnO_4$ samples with $0.5 \leqslant x \leqslant 1$ were prepared by solid state reaction in air, starting from stoichiometric amounts of CaO, Pr_6O_{11} and MnO_2, following the thermal treatment schematized in Fig. 1a.

*Corresponding author. Fax: +33-231-95-1600.
E-mail address: richard.retoux@ismra.fr (R. Retoux).

0022-4596/03/$ - see front matter © 2002 Elsevier Science (USA). All rights reserved.
doi:10.1016/S0022-4596(02)00124-X

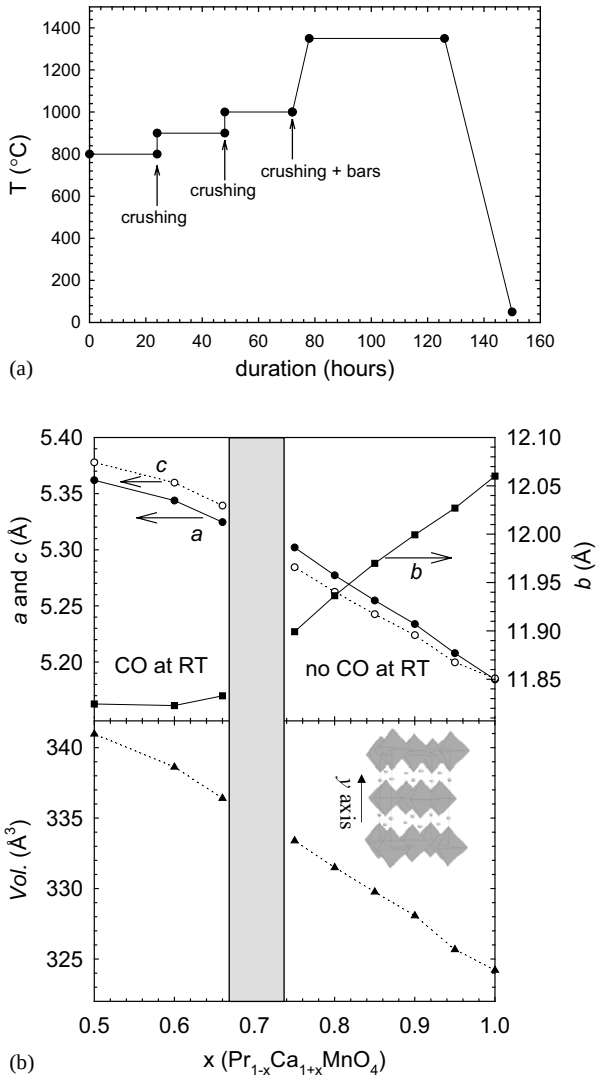

Fig. 1. (a) Schema of the thermal treatment used for the preparation of the $Pr_{1-x}Ca_{1+x}MnO_4$ samples. (b) x dependence of the lattice parameters (upper part) and volume (lower part), observed at room temperature. The gray area corresponds to the compositions where the charge ordering is not well established at RT. A schematized structure is also given in inset of the lower panel.

X-ray data were recorded at room temperature (RT) using a Philips diffractometer (Cu$K\alpha$ radiations in a $10^\circ \leqslant 2\theta \leqslant 100^\circ$ angular range). These data showed that all the samples are single phases, they were refined in the *Cmca* space group using the pattern matching option of the Fullprof program in order to follow the lattice parameters versus cationic composition evolution (Fig. 1b).

Oxidometry, using Fe^{+2} back titration, led to the O_4 oxygen content (in the limit of the accuracy ± 0.02) except for the $x=1$ compound for which it was determined to be $O_{3.95}$ and the analyzed cationic compositions correspond to the nominal ones. In fact, all the compounds were characterized by electron diffraction (ED), HREM and energy dispersive spectroscopy (EDS). For each of them, numerous crystallites were characterized. The samples were prepared by crushing the grains in alcohol. The small flakes were deposited on a holey carbon film, supported by a copper grid. The reconstruction of the reciprocal space was carried out by tilting around the crystallographic axes with a JEOL 200CX electron microscope and the ED study versus T with a JEOL 2010 microscope, working between 92 and 450 K. The HREM study was carried out at room temperature with a TOPCON 002B microscope, working at 200 kV and having a spherical aberration constant of 0.4 mm. The theoretical images were calculated using a Mac Tempas program.

Resistivity of the samples ($2 \times 2 \times 10$ mm) was measured by a standard four-probe technique. Magnetization data were collected with a SQUID magnetometer Quantum Design.

3. Results and discussion

3.1. Electron diffraction versus temperature

Three compositions ($x=0.67$, 0.6 and 0.5) have been studied by ED as a function of temperature. All of them are characterized by complex ED patterns, exhibiting at 92 K an incommensurate modulated structure, with $a \approx a_p\sqrt{2} \approx 5.3$ Å, $b \approx 12$ Å and $c \approx 1/qa_p\sqrt{2}$ (a_p being the ideal perovskite parameter cell). The amplitude of the modulation vector q decreases as x increases (Table 1) from $q=0.43$ for $x=0.5$ to $q=0.38$ for $x=0.67$ (to be compared to $q=0.28$ for $x=0.75$ [5]). The complexity of the ED patterns is due to the existence of twinning domains, on the one hand, and to the existence of three sets of reflections, which evolve with T, on the other hand.

One example of [0 1 0] patterns recorded at 92 K is given in Fig. 2a, for $x=0.67$. The most intense spots correspond to the Bragg peaks of the ideal I-type tetragonal structure of the RP's-1 member [6]. The second system consists in weak spots (indicated by open white arrows) attesting of the lowering the symmetry of the RP's-1 cell. The relative intensity of these extra reflections depends on the selected crystallites, but the reconstruction of the reciprocal space revealed a lowered P-type symmetry. The third system corresponds to the

Table 1
CO parameters from ED studies

x	q at 92 K	q at RT	Mn^{3+} content
1	No	No	0
0.75	0.28	No	0.25
0.67	0.38	0.33	0.33
0.6	0.375	0.39	0.4
0.5	0.43	0.43	0.5

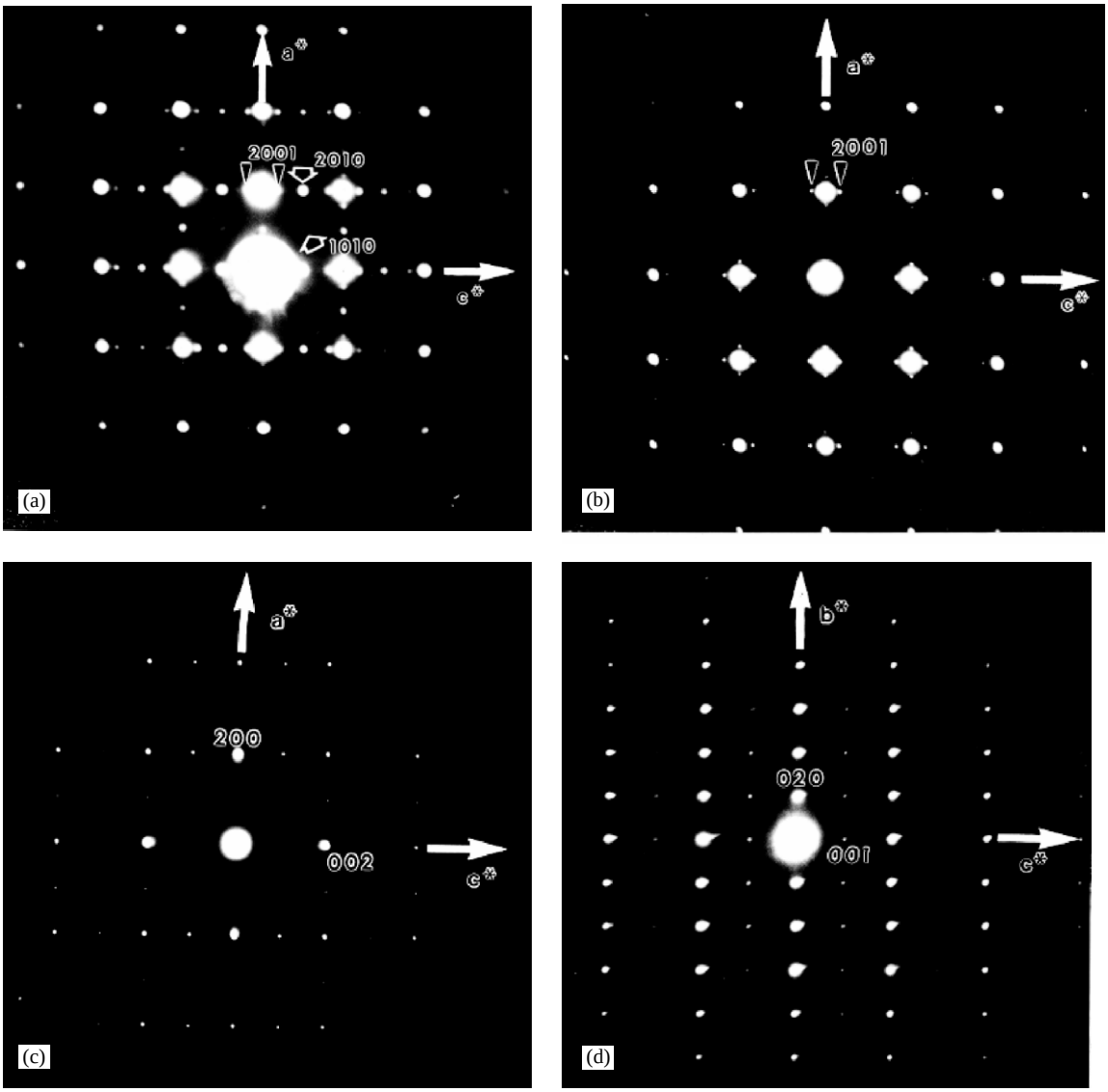

Fig. 2. $Pr_{0.33}Ca_{1.67}MnO_3$ [0 1 0] ED patterns registered at 92 (a), 250 (b) and 480 K (c) and [1 0 0] ED pattern recorded at 92 K (d).

weak spots indicated by black triangles, which are the satellites of the modulated structure, observed along the c^*-axis. The 2 0 0 1 reflection is indexed, using four $hklm$ indices. Tilting around c^* evidenced that the only condition limiting the reflection is $0klm$: $k=2n$ and $m=2n$. One example of [1 0 0] ED pattern is given in Fig. 2d.

By increasing the temperature, the intensity of the second system of extra reflections decreases dramatically. At $T\approx 250$ K, the reconstruction of the reciprocal space showed a structural transition from the P-type cell to the orthorhombic *Cmca* cell. This transition is especially visible through the disappearance of the extra 1 0 1 0 reflection, as illustrated in Fig. 2b (the 1 0 1 0 reflection totally disappears). The transition is smooth, the intensity of the 1 0 1 0 reflection starting to decrease at about 200 K. The third system of satellites is still observed, the q value being roughly constant. At this point, the modulated structure is C-type similar to that previously reported for $Pr_{0.25}Ca_{1.75}MnO_4$. Note that very weak extra reflections violating these conditions of reflection are sometimes observed in the [0 1 0] ED patterns, which have been correlated to micro-twinning phenomena as previously shown in other RP's-1 compounds [4,5].

At 300 K, the intensity of the satellites starts to decrease, the nodes are diffuse and become no more visible above T_{CO}, i.e. at $\approx$330–340 K. The reconstruction of the reciprocal space was then carried out at 480 K. The satellites have disappeared but the extra reflections characteristic of the orthorhombic distortion (*Cmca* space group) are weak but still visible (Fig. 2c).

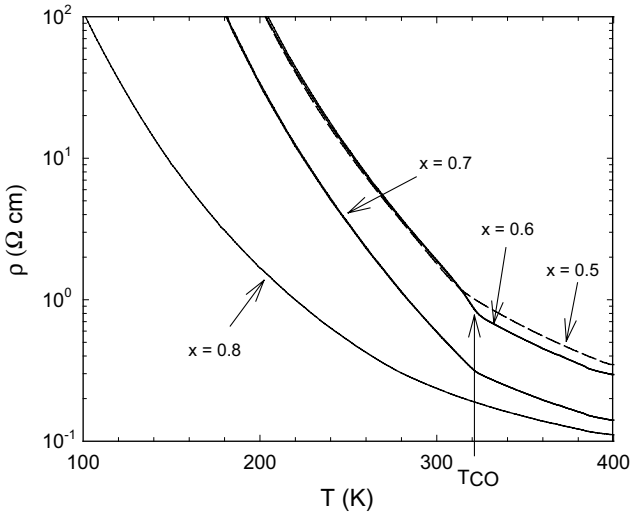

Fig. 3. $Pr_{1-x}Ca_{1+x}MnO_4$ resistivity curves [$\rho(T)$], the x values are given on the graph. T_{CO} is indicated by an arrow for $x=0.6$.

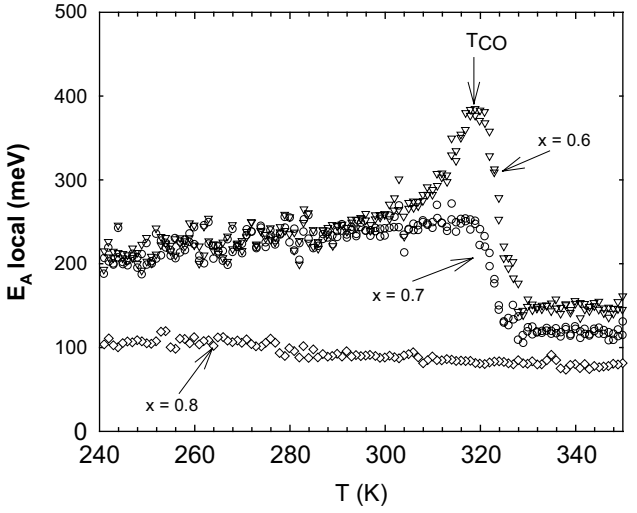

Fig. 4. Local activation energy versus temperature deduced from the $\rho(T)$ curves.

3.2. Evidence for charge–orbital ordering from magnetic and transport properties

The temperature dependence of the resistivity (ρ) (Fig. 3) confirms the existence of charge–orbital ordering for $0.50 \leqslant x < 0.80$. For this compositional range, one indeed observes a change of slope of ρ(T) around 250–330 K, depending on the x value, in agreement with the ED observations. The increase of the resistivity as x decreases below $x=0.8$ in the low-temperature region supports also the tendency of manganites with Mn valency ranging from +3.5 to +3.8 towards charge–orbital ordering in such RP's-1 compounds [1–3], as in perovskites [7]. The local activation energy $E_A^{local} = d\ln\rho/dT^{-1}$, plotted versus T (Fig. 4), confirms this viewpoint. It evidences for all the compounds with

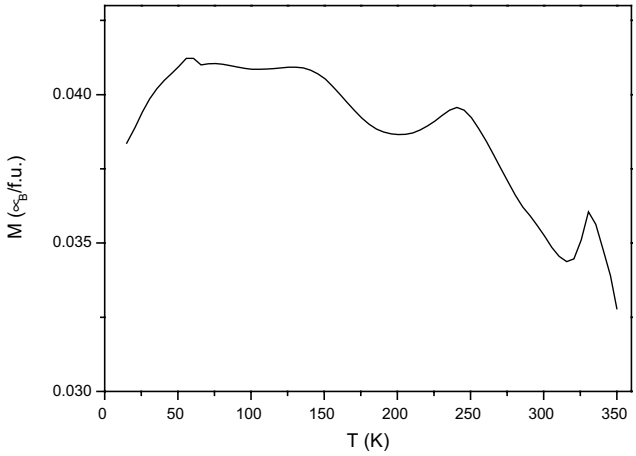

Fig. 5. Temperature dependence of the magnetization for $Pr_{0.4}Ca_{1.6}MnO_4$ ($x=0.6$).

$0.50 \leqslant x \leqslant 0.75$ a jump corresponding to the localization maximum which coincides with the change of slope on $\rho(T)$ and is characteristic of charge–orbital ordering. From these observations, it can be shown that T_{CO} increases from 275 K for $x=0.75$, goes through a maximum of 330 K for $x=0.60$ and then decreases to 310 K for $x=0.50$.

The strong interplay between charge and spins is confirmed by the T-dependent magnetization curves as exemplified for $x=0.60$ (Fig. 5). One indeed observes that this oxide exhibits a magnetic moment at 5 K smaller than 0.1 μ_B/f.u., suggesting an antiferromagnetic background state and a peak at $T_{CO} \approx 330$ K in agreement with the $\rho(T)$ evolution. Note, however, that the $M(T)$ curve is rather complex, with a maximum at 240 K which may be the signature of a change of sign for the magnetic fluctuations (paramagnetic regime) from $J>0$ for $T>T_{CO}$ to $J<0$ for $T<T_{CO}$, and a broad maximum extending from 135 to 57 K, the first temperature corresponding to T_N, according to neutron diffraction data [8]. Similar $M(T)$ curves are observed for all the charge-ordered compositions of the $0.50 \leqslant x \leqslant 0.75$ domain. This greater complexity of the $M(T)$ curves of those $Pr_{1-x}Ca_{1+x}MnO_4$ phases, compared to the perovskites $Pr_{1-x}Ca_xMnO_3$, originates probably from their 2D character which may enhance the magnetic fluctuations as previously mentioned in several antiferromagnetic K_2NiF_4-type compounds [9].

3.3. High-resolution electron microscopy: evidence for stripes at room temperature

The HREM characterization of the different samples ($0.5 \leqslant x \leqslant 0.75$) showed that they are well crystallized and defect free.

Viewing the crystallites along a direction perpendicular to the stacking b-axis confirms the RP's-1 structural type. A [1 0 0] HREM image is shown in

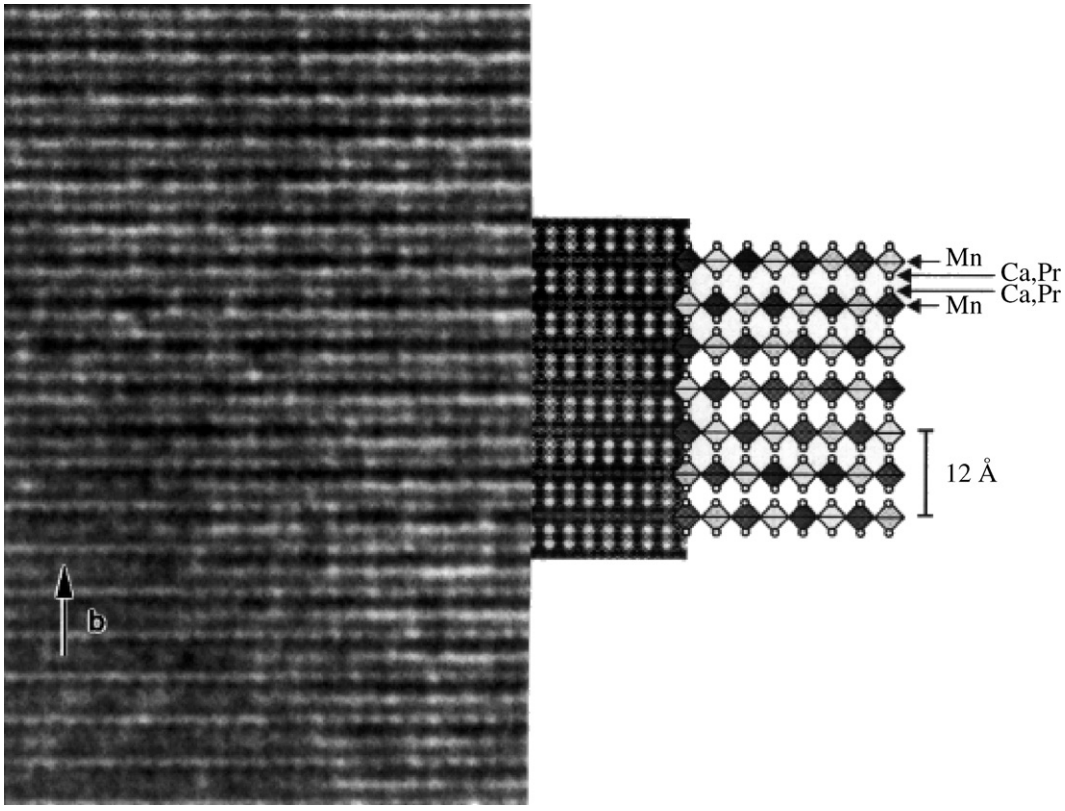

Fig. 6. $Pr_{0.33}Ca_{0.67}MnO_4$: RT [1 0 0] HREM image (left part), simulated image (middle part) and drawing of the structure (right part).

Fig. 6 (left part); the contrast consists in two adjacent rows of bright dots, correlated to the (Ca, Pr) positions of the double [*A*O] layers, sandwiching one row of small gray dots, correlated to the Mn positions (Fig. 6, right part). The simulated image, calculated for a focus value of –600 Å and a crystal thickness of 32 Å, is compared in the middle part (Fig. 6).

The [1 0 0] orientation does not provide any information on the charge-ordering phenomena, in agreement with ED observations ($0\,k\,l\,m$: $k=2n$ and $m=2n$). On the contrary, viewing the crystallites along the stacking *b*-axis showed that all the images are characterized by a striped contrast. For the $x=0.67$ sample, the modulation of the contrast is not very stable under the electron beam. It disappears rather quickly (as well as the satellites in the ED patterns) and the contrast is that of a non-modulated *Cmca*-type structure. On the contrary, the modulated structure of the $x=0.5$ compound is stable under the electron beam and the [0 1 0] HREM images, recorded at room temperature, clearly show the incommensurate character of the structure. One example of crystallite exhibiting two oriented domains (note 1 and 2 in the lower part of Fig. 7a) with perpendicular *c*-axes is displayed in Fig. 7a.The twinning boundary is roughly parallel to the [1 0 1] direction of the C-type orthorhombic cell. The zone of light electron density are highlighted and the cation positions are imaged as dark dots, each of these types of spots being theoretically evenly highlighted in an ideal RP's-1 structure. The modulation of the contrast results from the formation of double rows of spots (for a periodicity $2a_p\sqrt{2}\approx 5.3$ Å) running along a, the direction perpendicular to the modulation *c*-axis. In each double row, two adjacent dots are of equal intensity but the intensity of the successive pairs varies, inducing the modulated contrast (the intensity of the different rows varying indeed with the focus value and the crystal thickness). In this example, the double rows of darker dots (indicated by black arrows) alternate with one or two double rows of less dark dots (indicated by white strokes). Varying the focus value, the striped contrast, due to the formation of double rows, remains the main characteristic of the images. An example of enlarged image is given in Fig. 7b for a focus value where the cation positions are highlighted (the double rows are indicated by black arrows). The contrast can also be described through the alternation of double rows of bright ($5.3\approx 2a_p/\sqrt{2}$ large), with double ($5.3\approx 2a_p/\sqrt{2}$ large) or two double rows ($10.6\approx 4a_p/\sqrt{2}$ large) of brighter dots, perpendicular to the modulation direction. At grazing incidence viewing, the images show that the variation of contrast is associated to tiny atomic displacements, especially along the direction perpendicular to *c*. These arrangements of the double rows and the resulting periodicities,

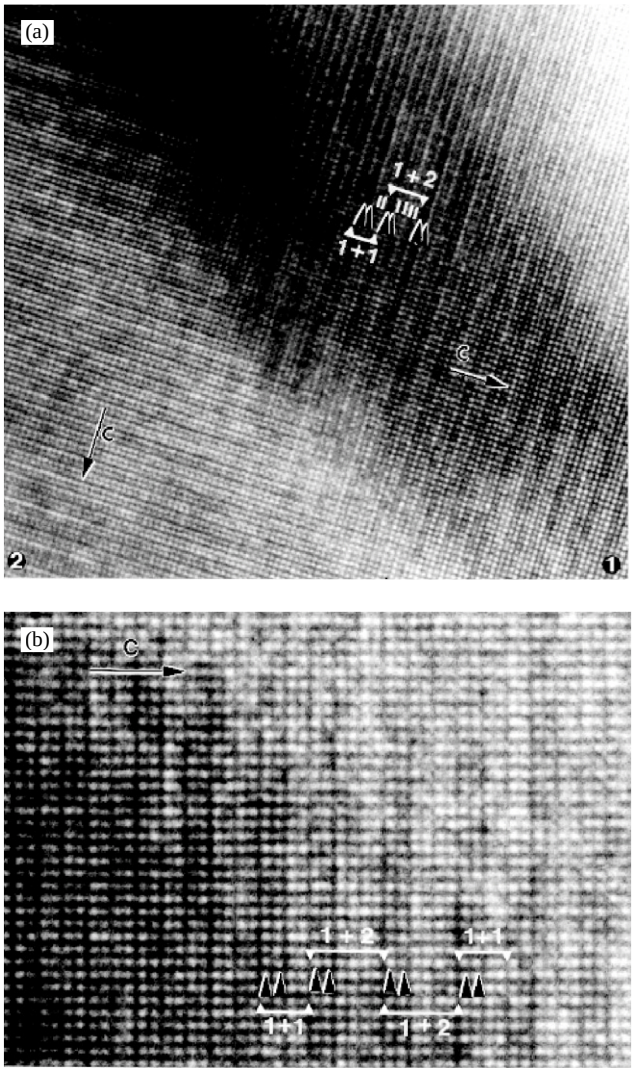

Fig. 7. $Pr_{0.5}Ca_{1.5}MnO_4$: RT [0 1 0] HREM image (a) and enlarged image (b).

(5.3 + 5.3 Å) for 1 + 1 double rows and (5.3 + 10.6 for one double + one quadruple rows) are consistent with the combination of two commensurate superstructures, namely $q = 0.5$ and 0.33, respectively. The larger proportion of the first sequence 1 + 1 double rows for $q = 0.5$, compared to the second one ($q = 0.33$), is in agreement with the incommensurate $q = 0.43$ value, which results from the arrangement of commensurate members (1/3 and 1/2).

In contrast to the 3D perovskites, these [0 1 0] images cannot be directly interpreted in terms of columns of one single kind of atom, since the Mn and Ca(Pr) positions are projected over the same point along *b*, as well as the oxygens of the rock-salt layers with the oxygens of the basal plane of the octahedra. As a consequence, it is not straightforward to propose a structural model based on a one-to-one correspondence between the contrast and the atomic positions. However, the ED and HREM studies provide important informations that one can analyze. First, the absence of visible satellites in the [1 0 0] ED patterns (and consequently of modulated contrast in the corresponding images) is consistent with the hypothesis of a displacive modulation perpendicular to c. The second important point is that the image contrast made of only double rows over long range, without deviation of this parity. This suggests that all the octahedral layers exhibit the same structure, built up from double stripes of manganese octahedra of one sort that alternate with double stripes ($q = 0.5$) or quadruple stripes of manganese octahedra ($q = 0.33$) of a second sort. Due to the K_2NiF_4 C-type structure, the projection along [0 1 0] can be described by the superposition of two kinds of layers (labeled 1 and 2 in Fig. 8) with a shift from $a/2$ or $c/2$. The observed contrast suggests that two successive ordered octahedral layers are shifted by $a/2$, with respect to each other, as schematized in Fig. 8 for the 1 + 2 contrast sequence. These two hypotheses (i.e. one pair sandwiched with one or two pairs in each (a,c) layer and coherence between layers along b) are built on the fact that the HREM images would not present perfect double row contrast over long distances (Fig. 7a) if one of these two characteritics is not satisfied. In particular, a shift of the ordered layers along c, instead a, does not allow to preserve such 1 + 1 and 1 + 2 contrasts.

Keeping in mind the translations of layers along *b*, the issue of the nature of the two kinds of Mn is not obvious. It is tempting to identify both kinds of stripes with Mn^{3+} and Mn^{4+} species. It is remarkable that, if *q* increases with the formal Mn^{3+} content (Table 1), this value of the modulation vector does not coincide with the Mn^{3+} content, suggesting that an ideal ordering, such as 1:1 or 1:2 or 1:3, between perfectly organized Mn^{3+} and Mn^{4+} stripes does not exist. In a more realistic way, the charge and orbital ordering in these systems may appear in the form of a partial delocalization, involving $Mn^{(3+\delta)+}$ and $Mn^{(4-\delta')+}$ stripes.

4. Concluding remarks

This study allows a phase diagram of the $Pr_{1-x}Ca_xMnO_4$ system to be presented (Fig. 9), shows that there exists a large composition range for the charge–orbital ordered state ($0.5 \leqslant x < 0.8$), in contrast to the weak ferromagnetic one ($0.8 < x \leqslant 1$). The charge–orbital ordering temperature T_{CO} of these oxides is remarkably high, from 300 to 330 K, the highest that has been observed to date in the 2D $(Ln,A)_2MnO_4$ manganites. In this respect, such a behavior is to be compared to the one observed for the $Bi_{0.5}Sr_{0.5}MnO_3$ and $Bi_{0.5}Ca_{0.5}MnO_3$ tridimensional perovskites, which exhibit high T_{CO} values, ≈ 500 K [10] and ≈ 330 K [11] respectively.

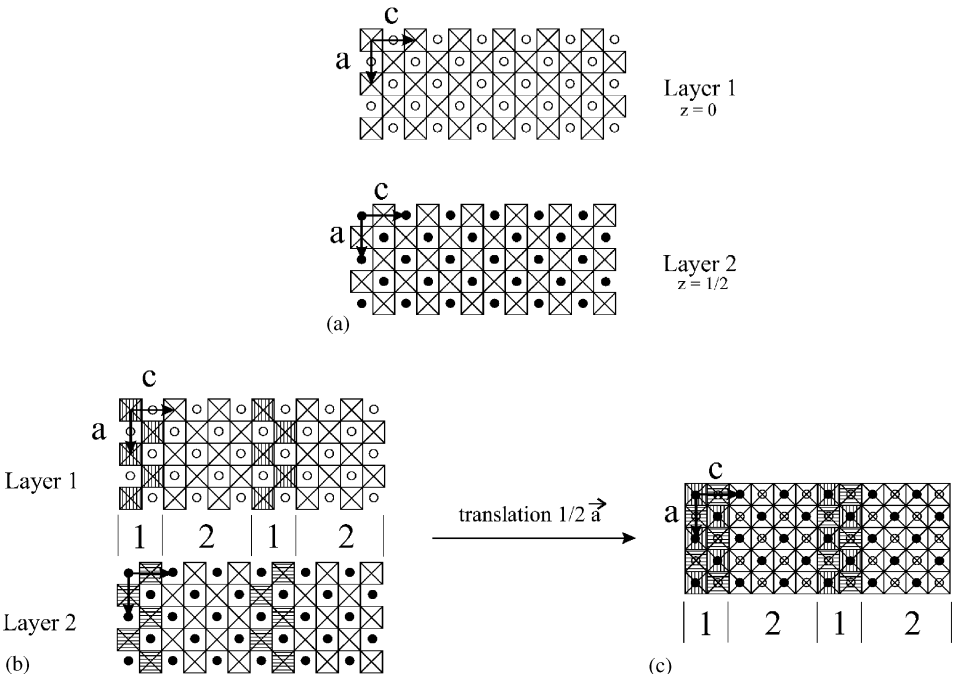

Fig. 8. Schematized model for the 1 + 2 sequence: (a) both types of perovskite layers projected along [1 0 1]. In the C-type orthorhombic structure, the translation between the perovskite layers stacked along [0 1 0] is either $a/2$ or $c/2$. (b) Same layers with charge–orbital ordering. (c) Projection of the structure along [0 1 0]. For clarity, open (○) and filled (•) circles are used for Sr atoms belonging to the layers 1 and 2, respectively.

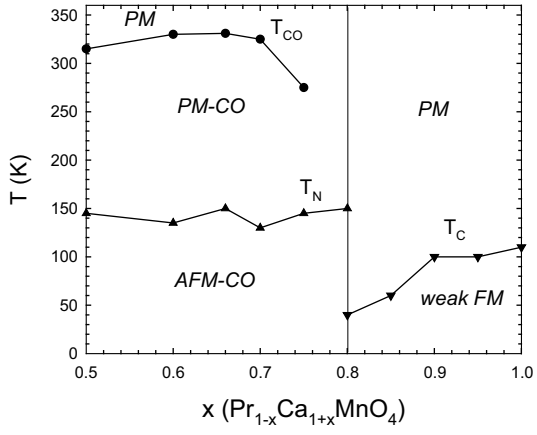

Fig. 9. $Pr_{1-x}Ca_{1+x}MnO_4$ magnetic phase diagram.

In this diagram, it is also remarkable, that there appears in the charge–orbital ordered domain a smooth (or diffuse) transition from P-type to C-type (*Cmca*) structures as T increases. Note that this structural temperature transition, close to 200 K, does not vary significantly with the composition, and also does not coincide with T_N, since the antiferromagnetic state appears below 150 K.

As for the bismuth 3D perovskites, the $Pr_{0.5}Ca_{1.5}MnO_4$ phase exhibits at low temperature a charge–orbital ordered structure involving two sorts of stripes, where the manganese valency remains an open question.

References

[1] C.N.R. Rao, P. Ganguly, K.K. Singh, R.A. Mohan Ram, J. Solid State Chem. 72 (1988) 14;
R.A. Mohan Ram, P. Ganguly, C.N.R. Rao, J. Solid State Chem. 70 (1987) 82.
[2] Y. Moritomo, Y. Tomioka, A. Asamitsu, Y. Tokura, Y. Matsui, Phys. Rev. B 51 (1995) 3297;
Y. Moritomo, A. Asamitsu, H. Kuwahara, Y. Tokura, Nature 340 (1996) 141.
[3] T. Kimura, K. Hatsuda, Y. Ueno, R. Kajimoto, H. Mochizuki, H. Yoshizawa, T. Nagai, Y. Matsui, A. Yamazaki, Y. Tokura, Phys. Rev. B 65 (2001) 020407.
[4] A. Maignan, C. Martin, G. Van Tendeloo, M. Hervieu, B. Raveau, J. Mater. Chem. 8 (1998) 2411.
[5] C. Autret, R. Retoux, M. Hervieu, B. Raveau, Chem. Mater. 13 (2001) 4745.
[6] S.R. Ruddlesden, P. Popper, Acta Crystallogr. 10 (1957) 538; 11 (1958) 54.
[7] M. Hervieu, A. Bamabé, C. Martin, A. Maignan, F. Damay, B. Raveau, Eur. Phys. J. B 8 (1999) 31.
[8] C. Autret, G. André, F. Bourée, C. Martin, M. Hervieu, A. Maignan, R. Retoux, B. Raveau, Appl. Phys. A, in press.
[9] G. Le Flem, Ph. Courbin, C. Delmas, J.L. Soubeyroux, Z. Anorg. Allg. Chem. 476 (1981) 69.
[10] J.L. Garcia-Munoz, C. Frontera, M. Aranda, A. Llobet, C. Ritter, Phys. Rev. B 63 (2001) 64415.
[11] V.A. Bokov, N.A. Grigorian, H.F. Bryzhina, Phys. Status Solidi 20 (1967) 745.